

NEUROSYSTEMS

Rebound spiking properties of mouse medial entorhinal cortex neurons *in vivo*

Yusuke Tsuno, George W. Chapman and Michael E. Hasselmo

Department of Psychological and Brain Sciences, Center for Systems Neuroscience, Center for Memory and Brain, Boston University, 2 Cummington Mall, Boston, MA 02215, USA

Keywords: h-current, oscillation, patch clamp, rebound potential, sag

Edited by Thomas Klausberger

Received 8 May 2015, revised 29 September 2015, accepted 5 October 2015

Abstract

The medial entorhinal cortex is the gateway between the cortex and hippocampus, and plays a critical role in spatial coding as represented by grid cell activity. In the medial entorhinal cortex, inhibitory circuits are robust, and the presence of the h-current leads to rebound potentials and rebound spiking in *in vitro* experiments. It has been hypothesized that these properties, combined with network oscillations, may contribute to grid cell formation. To examine the properties of *in vivo* rebound spikes, we performed whole-cell patch-clamp recordings in medial entorhinal cortex neurons in anaesthetized mice. We injected hyperpolarizing inputs representing inhibitory synaptic inputs along with sinusoidal oscillations and found that hyperpolarizing inputs injected at specific phases of oscillation had a higher probability of inducing subsequent spikes at the peak of the oscillation in some neurons. This effect was prominent in the cells with large sag potential, which is a marker of the h-current. In addition, larger and longer hyperpolarizing current square-pulse stimulation resulted in a larger probability of eliciting rebound spikes, though we did not observe a relationship between the amplitude or duration of hyperpolarizing current pulse stimulation and the delay of rebound spikes. Overall these results suggest that rebound spikes are observed *in vivo* and may play a role in generating grid cell activity in medial entorhinal cortex neurons.

Introduction

The medial entorhinal cortex (MEC) is the gateway between the cortex and hippocampus, and it plays a critical role in spatial coding and memory. It contains a variety of spatially modulated cells, including grid cells (Hafting *et al.*, 2005), conjunctive grid-by-head-direction cells (Sargolini *et al.*, 2006), and border cells (Solstad *et al.*, 2008). Grid cells are of particular interest due to the spatial influences in their response properties. Theta oscillations in the MEC, driven by medial septum cholinergic and GABAergic neurons, may be essential for generating grid cell activities (Brandon *et al.*, 2011; Koenig *et al.*, 2011). These theta oscillations may interact with inhibitory input, as stellate cells are mostly connected to each other via inhibitory interneurons, making a recurrent inhibitory network (Couey *et al.*, 2013). Stellate cells in MEC layer II have characteristic sag potentials and resonant frequency due to the h-current (Alonso & Llinás, 1989; Alonso & Klink, 1993; Haas & White, 2002; Giocomo *et al.*, 2007; Fernandez *et al.*, 2013), and this h-current can also elicit rebound potentials after inhibition (Alonso & Klink, 1993; Dickson *et al.*, 2000; Shay *et al.*, 2012). Pyramidal cells in the MEC also show sag potentials (Richter *et al.*, 1997, 2000), although they are much smaller than sag potentials in stellate

cells (Alonso & Klink, 1993). Post-inhibitory rebound spikes have also been observed in entorhinal inhibitory interneurons (Adhikari *et al.*, 2012). Thus, inhibitory input to MEC cells may elicit subsequent spikes due to rebound depolarizations that cause rebound spikes.

Rebound spikes may be integrated into a mechanism for generating theta cycle skipping (Jeffery *et al.*, 1995; Brandon *et al.*, 2013) and grid cell activity as demonstrated in a recent model (Hasselmo, 2014). The relationship between the amplitude or duration of hyperpolarizing current stimulation and the temporal delay of rebound spikes after stimulation has been described in *in vitro* recordings of MEC neurons (Ferrante *et al.*, 2014), suggesting a possible mechanism for regulating rebound spike timing by running speed. Recent studies also suggest that there is a relationship between the oscillation phase of hyperpolarizing current stimulation and subsequent spike probabilities at the peak of the oscillation in MEC layer II stellate cells in *in vitro* slice preparations (Shay *et al.*, 2015), suggesting a mechanism for phase precession and for maintaining select subpopulations of neurons active due to inhibition occurring at a specific phase of theta rhythm oscillations.

Thus, it is critical to examine the properties of rebound spikes of MEC neurons *in vivo*. In this study, we performed current-clamp recordings in MEC neurons *in vivo* from ketamine and xylazine-anaesthetized mice. To test the phase specificity of rebound spiking,

Correspondence: Yusuke Tsuno, as above.

E-mail: tsunosuke@gmail.com

we injected hyperpolarizing current stimulation superimposed on an artificial sine wave oscillation to mimic theta oscillations. We also used hyperpolarizing current square pulses with various amplitudes and durations to examine the relationships with the temporal delay of rebound spikes after stimulation. This study helps to fill the gap between the knowledge of slice experiments and the data on intact animals relevant to grid cell generation in freely moving animals.

Materials and methods

Animal surgery

Experiments were performed on 14 young adult C57BL6 male mice (age 4–14 weeks, 15–30 g; Charles River Laboratories) from which 16 successful neuronal recordings were used for analysis. Animals were anaesthetized with an intraperitoneal injection of ketamine [75 mg/kg body weight (kg bw)] and xylazine (15 mg/kg bw), or ketamine (75 mg/kg bw), xylazine (15 mg/kg bw) and acepromazine (2.0 mg/kg bw). Buprenorphine (0.05 mg/kg bw) was injected before craniotomy in some animals. Additional doses of ketamine and xylazine were given as needed (one-quarter of the initial dose) via injection cannula placed intraperitoneally. Body temperature was maintained at 37 °C with a heating pad. The depth of anaesthesia was monitored by tail pinch and the rhythm of breathing was also monitored during the entire experiment. Before surgery, bupivacaine (0.25%, 0.15 mL) was injected subcutaneously at the site of the incision. Each mouse was placed in a stereotaxic apparatus (SR-8N; Narishige) and prepared for acute electrophysiological recording from the MEC. Lubricant eye drops were placed on animals' eyes. After the incision, the surface of the skull was wiped with hydrogen peroxide and saline. Bregma and lambda were set at the same height, and a dental cement sheet was made on the surface of the skull with vetbond and metabond. The positions for craniotomies were marked for the hippocampus (posterior 2.2 mm, lateral 2.0 mm from bregma) and MEC (posterior 4.0 mm, lateral 3.7 mm from bregma). A craniotomy for the hippocampal electroencephalogram recording was made, and twisted teflon-insulated stainless steel electrodes (no. 790900; A-M Systems) were implanted vertically in the stratum radiatum of dorsal CA1 hippocampus (posterior 2.2 mm, lateral 2.0 mm from bregma; depth 1.4 mm from the surface) and secured in place using dental cement. A chamber was made with dental cement around the position of the craniotomy for MEC recording. An aluminium bar was implanted onto the skull with dental cement. A craniotomy (450–800 μm diameter) was made for patch-clamp recording from the MEC. A needle was used to remove the dura, and 1% agarose was put on the surface of the brain above the MEC to reduce pulsation, drying, and instability.

Ethical approval

All experiments were performed in accordance with experimental guidelines approved by the Institutional Animal Care and Use Committee at Boston University and The Animal Welfare Act.

Electrophysiology

In vivo patch-clamp recordings (Margrie *et al.*, 2002; Hahn *et al.*, 2012; Domnisoru *et al.*, 2013; Schmidt-Hieber & Häusser, 2013) were performed with patch electrodes created from glass capillaries (no. BF150-86-10; Sutter Instruments) on an electrode puller (P-97; Sutter Instruments). All recordings were performed in current-clamp

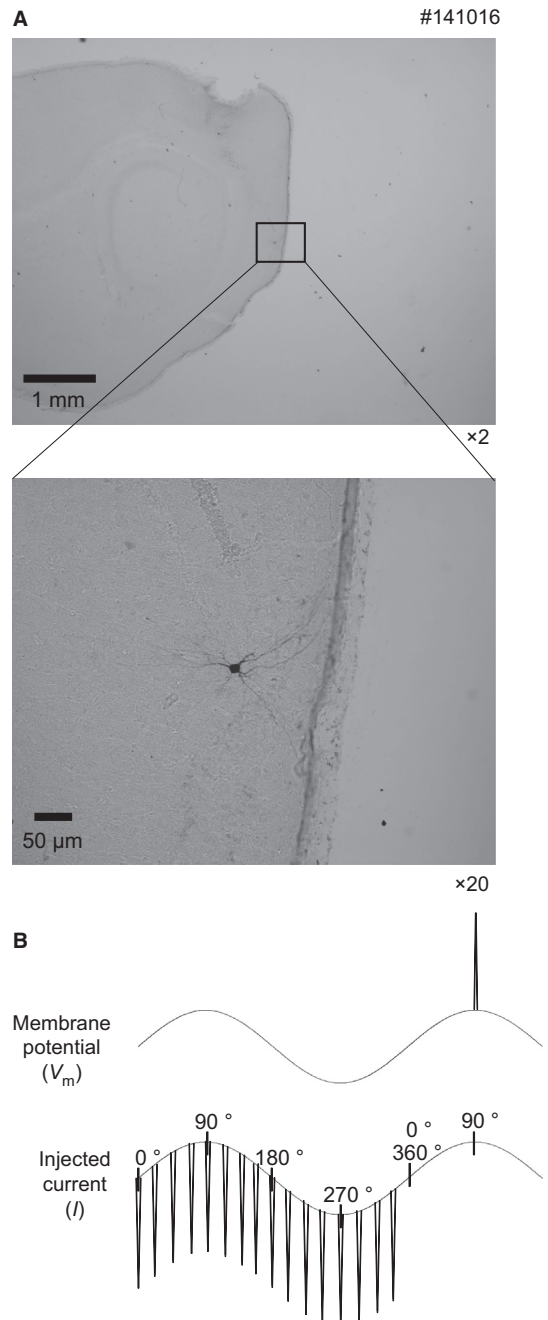


FIG. 1. Example of a biocytin-labelled cell and schematic diagram of the hyperpolarizing current stimulation in the oscillation. (A) One example of a recorded cell (parasagittal section). The biocytin-labelled cell is a stellate cell in layer II of the MEC. (B) Schematic diagram of the hyperpolarizing current stimulation superimposed with sinusoidal current input. Hyperpolarizing current stimulation is performed at 16 different phases of the oscillation, and subsequent spikes after the current stimulation are detected. The peak of the oscillation is 90°, and the trough is 270°.

mode. Pipettes were filled with an internal solution containing (in mM): 130 K-gluconate, 10 HEPES, 4 Mg-ATP, 7 KCl, 0.3 Na₂-GTP and 10 Na₂-phosphocreatine (pH adjusted to 7.25 with KOH, 285 mOsm). In addition, 0.5% biocytin was included in the internal solution for labelling. The filled pipette resistances were 3.8–7.5 M Ω . An Ag–AgCl reference electrode was placed outside the craniotomy, submerged in extracellular saline containing (in mM): 150 NaCl, 2.5 KCl and 10 HEPES, pH 7.4 (Domnisoru *et al.*,

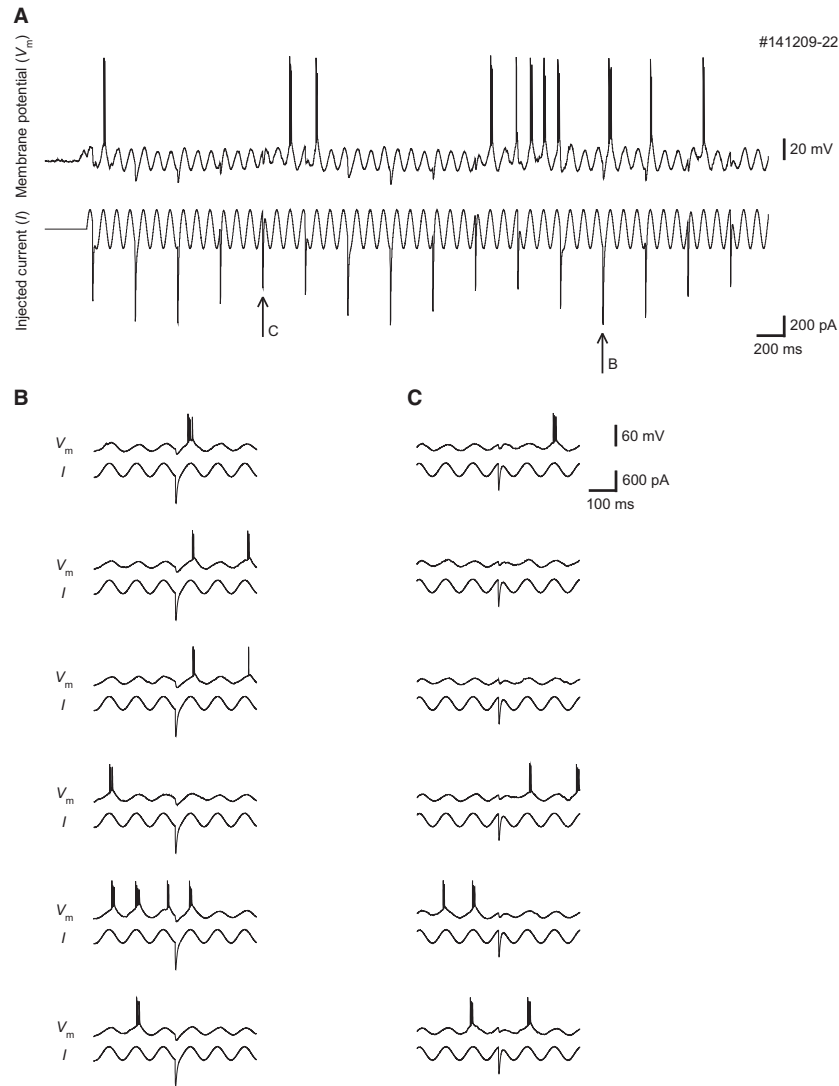
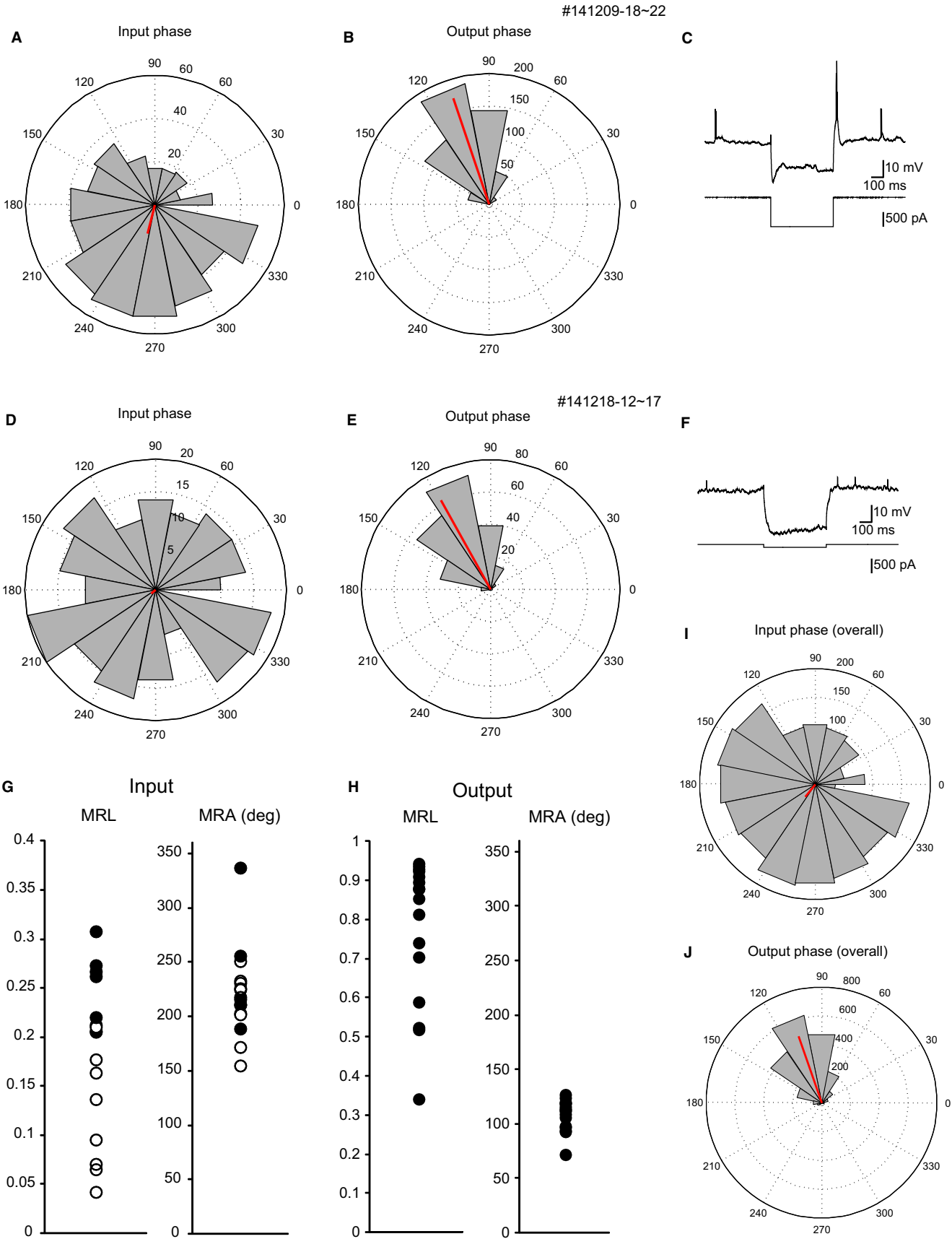


FIG. 2. Probability of subsequent spikes depended on the phase of the hyperpolarizing current stimulation in the oscillation. (A) Experimental design of hyperpolarizing current stimulation superimposed with sinusoidal current input. Hyperpolarizing current stimulation was performed on every third cycle of the sinusoidal current input shifting across 16 different individual phases of the oscillation. Upper trace: membrane potential. Lower trace: injected current. From the left, the phases are 157.5°, 225°, 292.5°, 360° (= 0°), 67.5° (with arrow C), 135°, 202.5°, 270°, 337.5°, 45°, 112.5°, 180°, 247.5° (with arrow B), 315°, 22.5° and 90°. By using this stimulation, the effect of the input phase of hyperpolarizing current stimulation on induction of subsequent spikes was evaluated. (B) Six examples of subsequent spikes induced in response to a specific input phase (247.5°, arrow B in A) of hyperpolarizing current injection. Counted spikes are (from top): 4, 2, 2, 0, 3 and 0 (11 spikes in total). (C) Six examples of subsequent spikes induced in response to another specific input phase (67.5°, arrow C in A) of hyperpolarizing current injection. Counted spikes are (from top): 0, 0, 0, 2, 0 and 3 (five spikes in total).

FIG. 3. Hyperpolarizing current stimulation at specific input phases of the oscillation increased the probability of subsequent spikes at the peak of the oscillation in some neurons. (A) Polar plot of the input phase of hyperpolarizing current stimulation that elicited subsequent spikes of a putative MEC layer II stellate cell. We defined this as the input phase for elicited spikes. The thick line indicates the MRL (0.26) and MRA (256°). Hyperpolarizing inputs that occur at the later descending phase of the oscillation (180–270°) tend to elicit subsequent spikes in this cell. This cell showed significant non-uniformity of the input phase for inducing spikes (Rayleigh test, $P = 1.18\text{E-}17$, including five recording trials, 552 spikes in total). (B) Polar plot of the output phase where spikes occur in the same neuron as in A. We defined this as the output phase of elicited spikes. The thick line indicates MRL (0.91) and MRA (109°). Spikes tend to occur at the peak of the oscillation. This cell showed significant non-uniformity of the output phase (Rayleigh test, $P = 5.32\text{E-}281$, five recording trials, 552 spikes in total). (C) Averaged trace of the response to hyperpolarizing current square pulse ($n = 5$) of the cell in A and B. Normalized sag amplitude was 0.38. (D) A different example neuron for which input phase did not show input phase relationship for inducing subsequent spikes. This cell was in MEC layer II or III with a small sag potential. This cell did not show significant non-uniformity of the input phase (MRL, 0.04; MRA, 218°; Rayleigh test, $P = 0.67$, six recording trials, 226 spikes in total). (E) Output phase of the neuron in D. This cell showed significant non-uniformity of the output phase (MRL, 0.88; MRA, 119°; Rayleigh test, $P = 7.43\text{E-}103$, six recording trials, 226 spikes in total). (F) Averaged trace of the response to hyperpolarizing current square pulse ($n = 10$) of the cell in D and E. Normalized sag amplitude was 0.09. (G) Plots of MRL and MRA of the input phase for eliciting spikes in all 16 neurons. Filled circles indicate the data that showed significant non-uniformity of the input phases that induced subsequent spikes (Rayleigh test with Bonferroni correction for multiple comparison, $P < 0.05/16 = 0.003125$). Open circles indicate the data that did not show significant non-uniformity. (H) Plots of MRL and MRA of output phase in all 16 neurons. All data showed significant non-uniformity of the output phase (filled circles, Rayleigh test with Bonferroni correction for multiple comparison, $P < 0.003125$). (I) Input phase of overall population (MRL, 0.16; MRA, 233°; Rayleigh test, $P = 9.41\text{E-}25$, 55 trials, 16 neurons, 2228 spikes in total). (J) Output phase of overall population (MRL, 0.79; MRA, 109°; Rayleigh test, $P < 2.23\text{E-}308$, 55 trials, 16 neurons, 2228 spikes in total).



2013). The liquid junction potential (14.0 mV) was corrected. Electrodes were angled at 14° from vertical, pointing to posterior. The electrode was lowered to the MEC (posterior 4.0 mm, lateral 3.7 mm from bregma, angled 14° to posterior, depth 1.9–2.6 mm from surface) by a micromanipulator (MP-225; Sutter Instruments). The manual blind patch recording was performed using the method as described previously (Kodandaramaiah *et al.*, 2012; Domnisoru *et al.*, 2013; Schmidt-Hieber & Häusser, 2013). Briefly, high positive pressure of > 200 mbar was used for the penetration going just above the target, and then the positive pressure was reduced to 25 mbar. The pipettes went down with 2- μ m steps. The positive pressure was released when the resistance increased more than 0.3 M Ω within 4 μ m. A suction pressure of –20 mbar was then applied, and the membrane potential was held at –30 mV. The potential was decreased to –40 mV, and the suction pressure was released. The potential was slowly lowered to –70 mV, and a giga-seal was formed. A suction pressure of –20 mbar and an electronic buzz were then applied to rupture the cell membrane. If the break-in was successful, capacitance compensation and bridge balance were set, and membrane potential recording began. The membrane potential and hippocampal electroencephalogram signal were amplified by Multiclamp 700B (Molecular Devices) and stored via an analog-to-digital converter (Digidata 1440A; Molecular Devices) with pCLAMP software (sampling rates: 10 kHz). Mechanical noise was reduced by use of an air table. Only recordings with resting membrane potentials more hyperpolarized than –54 mV (–68.9 \pm 5.2 mV, mean \pm SD) and spike peaks higher than –34 mV (7.7 \pm 25.2 mV) were used for analysis. Nine out of 16 cells showed overshooting spikes above zero. All spike amplitudes were greater than 20 mV (53.7 \pm 21.9 mV). During recording, the respiration rhythm was monitored by pressure sensor (MLT 1010; AD Instruments). In most cases, tonic negative current was injected to reduce spontaneous firing and to set membrane potential to perithreshold (–50 to –200 pA; –103 \pm 56 pA, mean \pm SD). By injecting this negative tonic current, resting membrane potentials were slightly hyperpolarized from –68.9 \pm 5.2 to –73.8 \pm 7.2 mV, and the spontaneous firing rate decreased from 5.7 \pm 5.5 to 0.4 \pm 1.0 Hz (mean \pm SD). Resting membrane potentials were measured at the trough of slow-wave oscillation, if slow-wave oscillations were observed. The duration of successful recordings was 26.4 \pm 9.8 min (mean \pm SD). If a drift of the baseline membrane potential occurred, the actual membrane potential was estimated by the assumption of a linear drift.

Stimulation

To measure the phase specificity of the capability of inhibitory inputs to elicit subsequent spikes, we superimposed a realistic hyperpolarizing synaptic current on a sinusoidal oscillatory input within MATLAB. Synaptic inputs were constructed with two exponential terms to mimic the time course of the synaptic current where fast and slow time constants were $\tau_1 = 1$ ms and $\tau_2 = 5$ ms, respectively.

$$I = e^{(-t/\tau_1)} - e^{(-t/\tau_2)}$$

The hyperpolarizing current was scaled so that the maximum amplitude was equal to twice the peak-to-peak voltage of the oscillatory signal. Hyperpolarizing current stimulation occurred at intervals of three cycles of the sinusoidal oscillation, and had 16 different phases (Figs 1B and 2A). All cells were run with either 8 or 10 Hz sinusoids, which is based on the resonance frequency of stellate cells in MEC layer II *in vivo* (Tsuno *et al.*, 2013). Each cell was also run

with peak-to-peak amplitudes of either 100, 200, or 400 pA, depending on the input resistance of each cell. Each recording trial was 40 s long and contained 30 s of sinusoid oscillations with hyperpolarizing input pulses, including five or six repeats of each set of 16 phases of hyperpolarizing input pulses. Between one and six recording trials were performed. Hyperpolarizing step currents were generated in pCLAMP. For the analysis of overall firing frequency, sinusoidal oscillation input without hyperpolarizing input pulses was performed. In these tests, the recording trial was 20 s long and contained 15 s of sinusoid oscillation without hyperpolarizing input pulses.

Histology

After the completion of each experiment, animals were deeply anaesthetized by ketamine (75 mg/kg bw) and xylazine (15 mg/kg bw), and perfused with saline and 10% formalin. The brains were extracted and postfixed with formalin over 24 h, and then placed in 30% sucrose for cryoprotection. The brains were sliced parasagittally into 80- μ m-thick sections by a cryostat (Leica). Biotin-labelled cells were visualized by avidin–biotin complex [VECTASTAIN Elite ABC kit (Standard), no. PK-6100; Vector] and 3,3'-diaminobenzidine reactions (DAB Peroxidase Substrate Kit, no. SK-4100; Vector). The sections were mounted on gelatin-coated slides and counterstained with Neutral Red.

We used histological information to determine the layer of the recorded cells in the MEC. However, cell type was not determined by histology because of the lack of labelling of dendrites in our experimental condition in most neurons. Out of 16 recorded cells, the soma and dendrites were labelled in two cells. In six cells, the soma was labelled, although the dendrites were not labelled. In seven cells, multiple cells were labelled probably because of the leak of internal solution. In this case, the layer of the recorded cell was estimated by the position of the multiple-labelled cells. In one cell, no cell was labelled, although the track trace was visible. From the track trace, the layer of the recorded cell was estimated. Out of 16 recorded cells, six cells were in MEC layer II, four cells were in layer II or III, four cells were in layer III, one cell was in layer III or V, and one cell was in layer V. Five out of six layer II cells showed a characteristic large-amplitude sag potential. These cells are considered to be putative stellate cells in MEC layer II, although we do not exclude the possibility that they are non-stellate cells.

Sag analysis

Hyperpolarizing square-current injection was delivered to examine the sag amplitude of each cell. The amplitude of the hyperpolarizing current was –100, –200, –500, or –1000 pA, and the duration was 500 or 1000 ms. Between one and 15 traces were averaged and used for the sag analysis. The raw sag amplitude was calculated by the difference between the voltage of the peak hyperpolarization elicited by hyperpolarizing square current and the steady-state membrane potential during the hyperpolarizing current. The normalized sag amplitude was calculated as the raw sag amplitude divided by the peak hyperpolarization amplitude. The input resistance was calculated as the peak hyperpolarization amplitude divided by the amplitude of the hyperpolarizing square current. The membrane potential just before the hyperpolarizing square current was between –56 and –78 mV.

Data analysis

All data were recorded by pCLAMP software, and exported to MATLAB for analysis. For sinusoidal inputs, action potentials

were found as the peak membrane potential in any 20 ms period reaching at least -25 mV. Output phases were identified as the phase of the baseline oscillation of the current at the time of the spike potential. Input phases were calculated as the phase of the most recent current input previous to an action potential, with the additional requirement that the input was within two cycles of the oscillation. In the case of bursting activity (Fig. 2B), all spikes of the burst were included for analyses. Phases were defined based on the sinusoid function, putting 90° at the peak of the input, 270° at the trough, 0° at the zero-crossing on the ascending phase, and 180° at the zero-crossing on the descending phase of the injection. The sinusoid strength was adjusted as in Materials and methods, leading to at least 30 spikes for each cell. The degree of non-uniformity was determined by the mean resultant length (MRL), and the preferred angle was calculated with the mean resultant angle (MRA) (Berens, 2009). Tests of non-uniformity were performed with the Rayleigh test included in the MATLAB circular statistics toolbox (Berens, 2009), by which the z-score and *P*-value were calculated. The Pearson correlation was used for the analysis of linear regression. To examine the overall firing frequency induced by sinusoidal input with or without hyperpolarizing current input, the probability of more than one spike in each sinusoidal oscillation cycle was calculated. The phases of these spikes in the oscillation were also calculated. A two-sided Wilcoxon signed-rank test was used for comparing paired data, and a Watson–Williams test was used for comparing circular data.

Results

Difference of subsequent spike probability due to the phase of hyperpolarizing current stimulation during sinusoidal input *in vivo*

In order to determine the feasibility of rebound spiking models of generating grid cells, we performed patch-clamp techniques in anaesthetized animals. Neurons in this study were confirmed to lie in layer II, III or V of the MEC, based on biocytin labelling or track traces of recording pipettes (Fig. 1A). Of 16 neurons, five were determined as putative MEC layer II stellate cells exhibiting clear large-amplitude sag potentials.

We used hyperpolarizing current stimulation with sinusoidal input to elicit subsequent spikes (Figs 1B and 2A). Hyperpolarizing current stimulation occurred in 16 different phases of the sinusoidal oscillation. Raw traces of membrane potential at specific phases of hyperpolarizing input pulses are shown in Fig. 2B and C. We defined the input phase (Fig. 3A and D) as the phase of hyperpolarizing current stimulation that elicits subsequent spikes, and the output phase (Fig. 3B and E) as the phase of the occurrence of output spikes. A polar plot of the input phase of this putative MEC layer II stellate cell (normalized sag amplitude, 0.38) (Fig. 3C) combined from five recording trials showed that most hyperpolarizing input pulses that elicited spikes occurred at the latter descending phase (near the trough) of the oscillation (Fig. 3A) (Rayleigh test, $P = 1.18\text{E-}17$, 552 spikes in total). A polar plot of the output phase of this cell showed that most spikes occurred at the peak of the sinusoidal oscillation (Fig. 3B) (Rayleigh test, $P = 5.32\text{E-}281$, 552 spikes in total). Another cell, which was in MEC layer II or III with small sag potential (normalized sag amplitude, 0.09) (Fig. 3F), showed no clear input phase relationship (Fig. 3D) (Rayleigh test, $P = 0.67$, six recording trials, 226 spikes in total), although it showed a clear output phase relationship

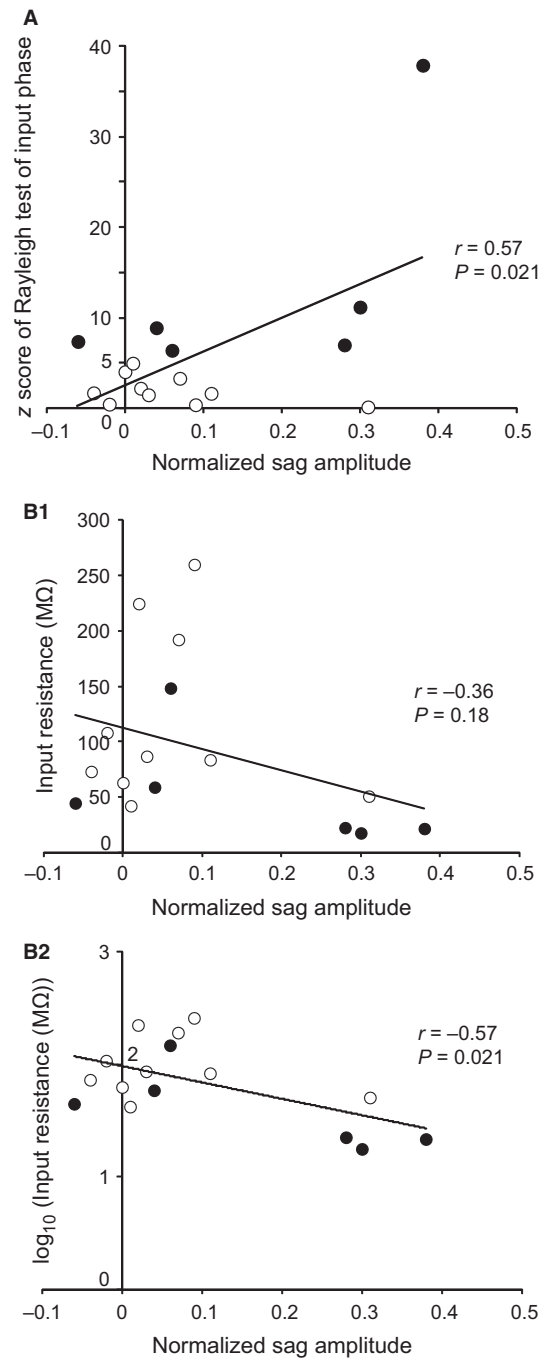


FIG. 4. Sag amplitude was correlated with input phase relationship. (A) The relationship between normalized sag amplitude and z-score of Rayleigh test of input phase in each cell ($n = 16$). Filled circles indicate the data that showed significant non-uniformity of the input phase in Fig. 3G. Open circles indicate the data that did not show significant non-uniformity of the input phase. (B) The relationship between normalized sag amplitude and input resistance (linear scale in B1 and log scale in B2) in each cell ($n = 16$). Filled and open circles indicate same properties as in (A).

(Fig. 3E) (Rayleigh test, $P = 7.43\text{E-}103$, six recording trials, 226 spikes in total). In total, six out of 16 neurons showed significant unimodal deviation from uniformity of the input phase (Rayleigh test with Bonferroni correction for multiple comparison, $P < 0.05/16 = 0.003125$). Five out of six neurons that showed a significant input phase relationship (Fig. 3G right, filled circles) had MRAs that were between 180° and 270° , which is the latter descending phase of

the oscillation. One neuron with a significant input phase relationship showed an MRA of 330° . These six neurons had MRLs that were larger than 0.2. Of the five putative MEC layer II stellate cells recorded in this dataset, three neurons showed a significant input phase relationship. In the other 11 cells, including MEC layer II, III, and V neurons without large sag potential (normalized sag potential was < 0.1), three neurons showed a significant input phase relationship. All 16 neurons showed significant unimodal deviation from uniformity of the output phase that tended to be at the peak of the oscillation (Fig. 3H) (Rayleigh test with Bonferroni correction, $P < 0.003125$). In evaluating the data from the overall population, the data showed both a significant input phase relationship (Fig. 3I) (Rayleigh test, $P = 9.41\text{E-}25$; MRL, 0.16; MRA, 233° ; 55 trials, 16 neurons, 2228 spikes in total) and a significant output phase relationship (Fig. 3J) (Rayleigh test, $P < 2.23\text{E-}308$; MRL, 0.79; MRA, 109° ; 55 trials, 16 neurons, 2228 spikes in total). These results indicate that spikes in all cells tended to occur at around the peak of the oscillation, whereas hyperpolarizing input pulses were most likely to elicit subsequent spikes if injected during the latter descending phase of oscillation.

Correlation between the normalized sag amplitude and input phase relationship

If the input phase relationship is because of the rebound potential and rebound spikes mediated by the sag potential and h-current, there should be a correlation between the magnitude of the sag potential and induction of the input phase relationship. To examine this, the normalized sag amplitude and z-score of the Rayleigh test, which tests the unimodal deviation from uniformity of the input phase relationship, were compared (Fig. 4A). There was a correlation between the normalized sag amplitude and z-score of the Rayleigh test of the input phase relationship ($r = 0.57$, $P = 0.021$, Pearson correlation). Thus, it is possible that the sag potential accounted for the input phase relationship. Also, stellate cells have a large sag potential and relatively low input resistance (Quilichini *et al.*, 2010). To examine the relationship between the sag potential and input resistance, they are compared in Fig. 4B1 and B2. There was a tendency for a larger normalized sag amplitude to be associated with lower input resistance. Although there was no significant linear correlation (Fig. 4B1) ($r = -0.36$, $P = 0.18$, Pearson correlation), there was significant correlation between the

\log_{10} value of input resistance and normalized sag potential (Fig. 4B2) ($r = -0.57$, $P = 0.021$, Pearson correlation). Four putative MEC layer II stellate cells that had large normalized sag potentials (> 0.25) (Fig. 4B1) also had low input resistance ($< 60 \text{ M}\Omega$). Three out of these four cells also showed significant deviation from uniformity of the input phase (filled circles in Fig. 4B1). However, three cells that showed significant deviation from uniformity of the input phase had a small normalized sag amplitude (< 0.1) (filled circles in Fig. 4A and B1).

Overall firing frequency was slightly decreased by hyperpolarizing current stimulation

To examine whether hyperpolarizing input pulses affected the overall firing frequency, we compared the probability of spikes in each oscillatory cycle with or without hyperpolarizing input pulses during sinusoidal oscillatory current stimulation in 11 out of 16 recorded neurons. The probability of more than one spike in each cycle of sinusoidal oscillation was slightly decreased by hyperpolarizing current inputs. As shown in Fig. 5A, the probability was 0.289 ± 0.091 (mean \pm SD) without hyperpolarizing current input, and 0.241 ± 0.119 with hyperpolarizing current input ($P = 0.042$, two-sided Wilcoxon signed-rank test for paired data, $n = 11$). The phases of spike firing were also compared between sinusoidal current stimulation with or without hyperpolarizing current input. There were no significant differences for both MRL and MRA. As shown in Fig. 5B, the MRL was 0.79 ± 0.19 without hyperpolarizing current input, and 0.83 ± 0.13 with hyperpolarizing current input ($P = 0.067$, two-sided Wilcoxon signed-rank test, $n = 11$). As shown in Fig. 5C, the MRA was $102.6 \pm 36.3^\circ$ (mean \pm circular SD) without hyperpolarizing current input, and $111.2 \pm 9.2^\circ$ with hyperpolarizing current input ($P = 0.467$, Watson–Williams test, $n = 11$) for spike phases in the oscillation.

Rebound spikes are elicited by strong and long-duration hyperpolarizing stimulation, but not by weak and short-duration hyperpolarizing stimulation

We also investigated how the amplitude and duration of hyperpolarizing input affected rebound spikes, using various durations and

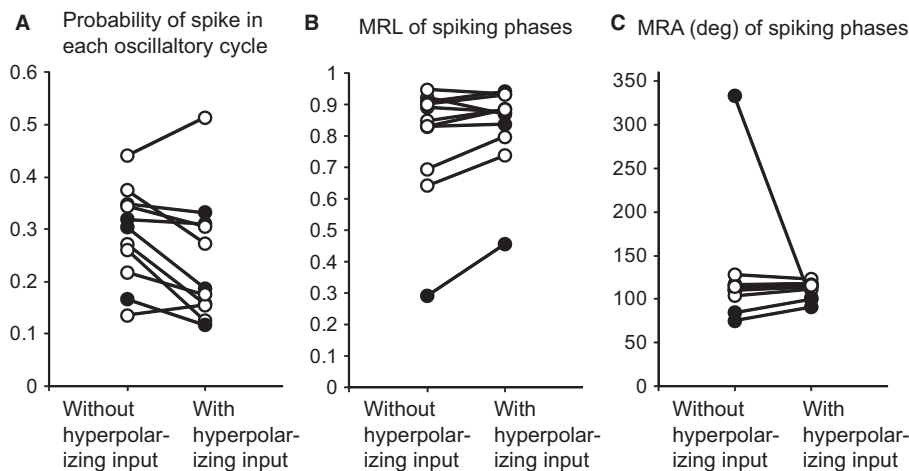


FIG. 5. Hyperpolarizing input pulses slightly decreased overall firing frequency and had almost no effect on output phases. (A) Probability of more than one spike in each sinusoidal oscillation cycle with or without hyperpolarizing current stimulation ($n = 11$). Filled circles indicate the data that showed significant non-uniformity of the input phase in Fig. 3G. Open circles indicate the data that did not show significant non-uniformity of the input phase. (B) MRL of phases of firing output in sinusoidal oscillatory input with or without hyperpolarizing current input ($n = 11$). Filled and open circles indicate the same as in (A). (C) MRA of phases of firing output in sinusoidal oscillatory input with or without hyperpolarizing current input ($n = 11$). Filled and open circles indicate the same as in (A).

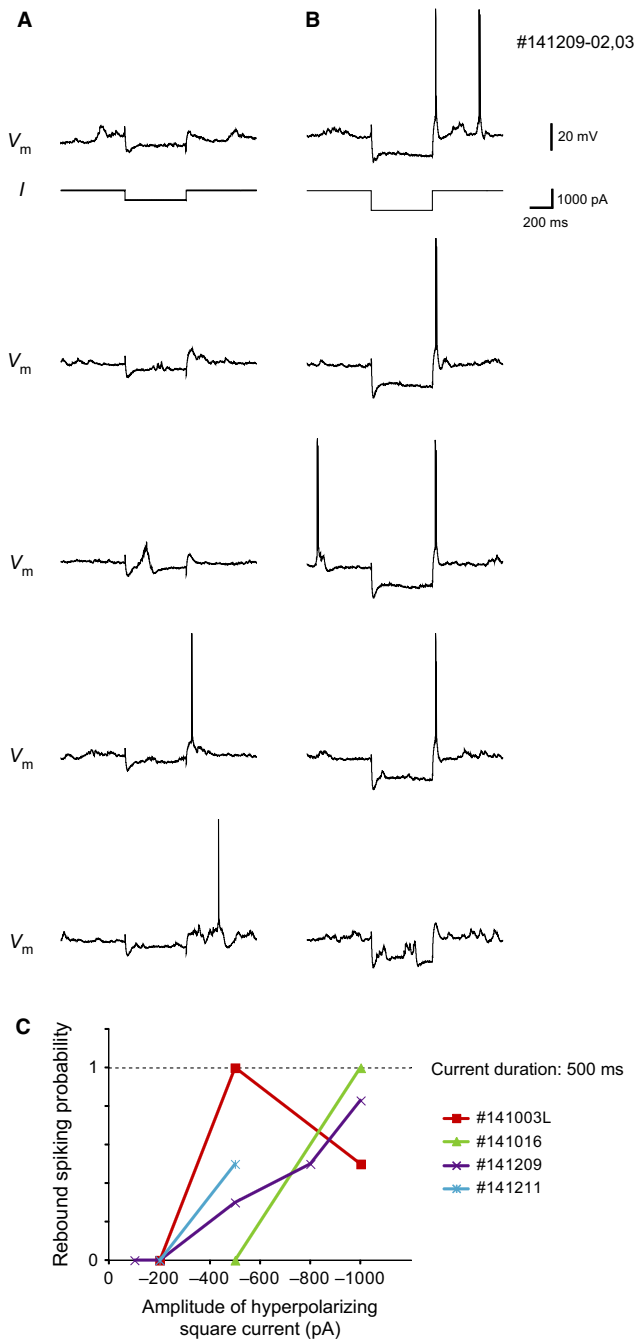


FIG. 6. Larger amplitude of hyperpolarizing current square-pulse stimulation had higher probability of eliciting rebound spikes. (A) Examples of rebound spikes with long (500 ms) and medium (-500 pA) hyperpolarizing current square-pulse stimulation in an entorhinal cortex neuron. In this example, two out of five hyperpolarizing current injections elicited rebound spikes. Membrane potential was between -59 and -69 mV. (B) Examples of rebound spikes with long (500 ms) and large (-1000 pA) hyperpolarizing current square-pulse stimulation in the same neuron as in (A). Four out of five hyperpolarizing current injections elicited rebound spikes. Membrane potential was between -59 and -69 mV. (C) Rebound spiking probability plot with different amplitude of hyperpolarizing current square-pulse stimulation in four cells. Duration of hyperpolarizing current stimulation is fixed at 500 ms.

amplitudes of square-pulse currents. Four out of 16 recorded neurons, including three putative stellate cells in MEC layer II, showed rebound spikes with hyperpolarizing current square-pulse stimulation in some cases. Figure 6A and B shows one neuron in

which -500 pA, 500 ms hyperpolarizing square-pulse stimulation elicited rebound spikes in two out of five trials (Fig. 6A); -1000 pA, 500 ms hyperpolarizing square-pulse stimulation elicited rebound spikes in four out of five trials (Fig. 6B). In all four neurons, there was a tendency for larger amplitude hyperpolarizing square-current stimulation to have higher rebound spiking probability (Fig. 6C). Figure 7A shows that short durations of hyperpolarizing stimulation (40, 50, and 80 s) did not often elicit subsequent spikes, although rebound potentials were observed. In contrast, longer durations of hyperpolarizing stimulation (500 and 1000 ms) elicited subsequent spikes with higher probabilities (Fig. 7A). In all four neurons, there was a tendency for longer duration hyperpolarizing square-current stimulation to have higher rebound spiking probability (Fig. 7B and C). We did not observe any trend between the amplitude or duration of the inhibition and the temporal delay to rebound spiking at the end of the square-current injection pulse.

Discussion

In the present study, we examined the property of rebound potentials and spikes *in vivo* using two stimulation methods, i.e. hyperpolarizing current stimulation along with sinusoidal oscillations and hyperpolarizing current square-pulse stimulation with various amplitudes and duration. By using hyperpolarizing current stimulation with sinusoidal oscillations, we found that there is a relationship between the phase of hyperpolarizing current stimulation and the probability of spikes at the peak of the oscillation after the stimulation. This indicates that hyperpolarizing input pulses at specific phases of the oscillation increase the probability of subsequent spikes. This can be explained by the rebound potential after the hyperpolarizing current stimulation. By using hyperpolarizing current square-pulse stimulation with various amplitudes and durations, we found that larger and longer duration hyperpolarizing stimulation has a higher probability of eliciting rebound spikes *in vivo*. We did not observe a relationship between the amplitude and duration of hyperpolarizing current pulse stimulation and the temporal delay of rebound spikes at the end of stimulation. These results contribute to the experimental evaluation of a model of grid cell activity incorporating oscillatory interference, resonance frequency, and theta cycle skipping (Hasselmo, 2014; Hasselmo & Shay, 2014).

Rebound spikes *in vivo*

Because of the predominance of inhibitory network interactions within layer II of the MEC (Dhillon & Jones, 2000; Couey *et al.*, 2013) and the h-current present in stellate cells (Dickson *et al.*, 2000; Heys *et al.*, 2010; Heys & Hasselmo, 2012; Tsuno *et al.*, 2013), it was proposed that inhibition enhances the excitation and firing of entorhinal neurons in a timely manner via rebound spikes (Hasselmo, 2014; Shay *et al.*, 2015). This possibility is supported by the current study of hyperpolarizing current stimulation with sinusoidal input *in vivo*. This study is the first report of the relationship between hyperpolarizing current input and subsequent spike probability during oscillatory input *in vivo*.

Although the overall firing frequency was slightly decreased by hyperpolarizing current stimulation, the cells that did not show an input phase relationship for inducing spikes showed a larger decrease of overall firing frequency (open circles in Fig. 5A) than the cells that showed an effect of input phase for inducing spikes (filled circles in Fig. 5A). Rebound potentials and rebound spikes

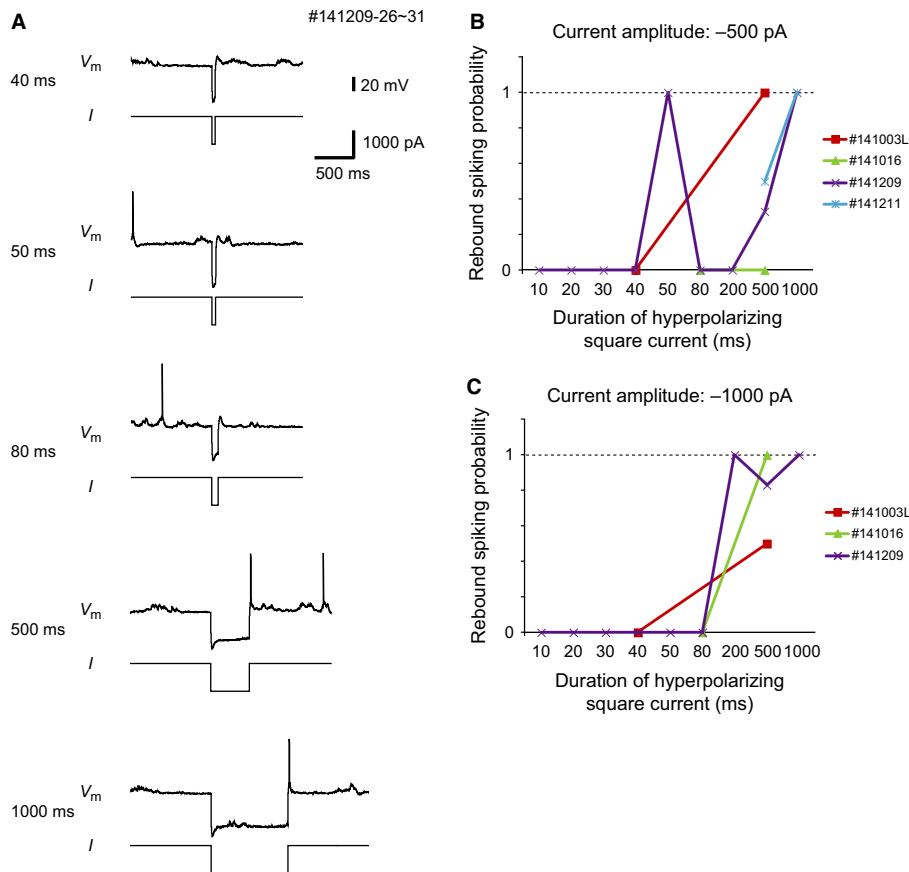


FIG. 7. Longer duration of hyperpolarizing current square-pulse stimulation had higher probability of eliciting rebound spikes. (A) Examples of rebound spikes with different duration (from top: 40, 50, 80, 500 and 1000 ms), of hyperpolarizing current square-pulse stimulation (-1000 pA) in an entorhinal cortex neuron. Note that hyperpolarizing stimulation with short duration (40, 50, and 80 ms) did not elicit rebound spikes, and hyperpolarizing stimulation with long duration (500 and 1000 ms) did elicit rebound spikes. Membrane potential was between -59 and -69 mV. (B) Rebound spiking probability plot with different duration of hyperpolarizing current square-pulse stimulation in four cells. Amplitude of hyperpolarizing current stimulation is fixed at -500 pA. (C) Rebound spiking probability plot with different duration of hyperpolarizing current square-pulse stimulation in three cells. Amplitude of hyperpolarizing current stimulation is fixed at -1000 pA.

probably increase firing frequency and compensate for the decrease of overall firing frequency in the neurons that showed an effect of input phase for inducing spikes. It is also possible that hyperpolarizing input pulses on later ascending phases (between 0° and 90°) decrease subsequent spike probability.

Spontaneous membrane potential fluctuations are observed in anaesthetized animals and in awake head-restrained animals (Domnisoru *et al.*, 2013; Schmidt-Hieber & Häusser, 2013; Y. Tsuno & M. E. Hasselmo, personal observation). These fluctuations of membrane potentials made it difficult to set the membrane potential to a perithreshold region *in vivo*, whereas the membrane potential is more easily controlled during *in vitro* experiments. Also, large fluctuations, including large intrinsic oscillations called slow waves, can make it difficult to observe rebound spikes. These difficulties in observing rebound spikes *in vivo* might be the reason for the lack of observation of a relationship between the amplitude or duration of hyperpolarizing current square-pulse stimulation and the temporal delay of the subsequent rebound spike, which was clearly shown in our *in vitro* study (Ferrante *et al.*, 2014).

We also observed an influence of input phase on spike induction in putative non-stellate cells. Some non-stellate cells in layer III and V of the MEC showed small sag potentials. Thus, small sag potentials generated by the h-current might affect the probability of rebound spikes and the influence of input phase on spike induction

in these neurons. Another possible cause of the influence of input phase on spike induction is the effect of some currents in which inactivation is released by hyperpolarization, such as the low-threshold Ca^{2+} current (McCormick & Huguenard, 1992; Lüthi & McCormick, 1998; Izhikevich, 2007). It is also possible that hyperpolarizing input pulses in the ascending phase of the oscillation inhibit subsequent spike firing and thereby affect the input phase relationship.

Function of rebound spikes

Our study suggests that the probability of rebound spikes increases if the hyperpolarizing input pulses come at specific phases of oscillation in the membrane potential. Stellate cells show intrinsic subthreshold membrane potential oscillations (Dickson *et al.*, 2000; Yoshida *et al.*, 2011), and the entorhinal cortex also receives oscillatory input from the medial septum (King *et al.*, 1998; Varga *et al.*, 2008) whose GABAergic projections regulate the activity of inhibitory interneurons in the entorhinal cortex (Gonzalez-Sulser *et al.*, 2014). These properties of rebound spikes and oscillation will help MEC cells to code spatial and temporal information in a timely manner. It was reported that there is a relationship between theta input and spike timing (Fernandez *et al.*, 2013), which is the output phase in our definition. Although this study analysed the influence

of voltage fluctuations, it did not focus on the induction of rebound spikes with hyperpolarizing input pulses.

Although there is evidence to support the possibility that MEC layer II stellate cells are grid cells (Burgalossi *et al.*, 2011; Domnisoru *et al.*, 2013; Schmidt-Hieber & Häusser, 2013), it was proposed that most of the grid cells are pyramidal cells in MEC layer II, and most border cells are stellate cells (Tang *et al.*, 2014; Ray *et al.*, 2014; Savelli & Knierim, 2014). In the study of Tang *et al.* (2014), the proportion of observed grid cells was low (19% in putative pyramidal cells and 3% in putative stellate cells) relative to other studies [50%; Sargolini *et al.* (2006), Boccara *et al.* (2010)], indicating that there are some discrepancies. Also, a recent study using Ca²⁺ imaging in freely moving mice showed that grid cell responses appeared in both stellate cells and pyramidal cells in similar proportions (Sun *et al.*, 2015). Although we need additional experimental evidence to make a conclusion, we also observed an input phase relationship for inducing subsequent spikes in some putative non-stellate cells. Rebound spikes may also have a critical role in pyramidal cells. It was reported that the sag potential mediated by the h-current was also observed in CA1 pyramidal cells in the hippocampus (Zemankovics *et al.*, 2010), and HCN1 knockout mice showed a significant change of place cell activity (Hussaini *et al.*, 2011). Also, a relationship between rebound spikes and synchronization was previously proposed in the hippocampus (Cobb *et al.*, 1995). It may be possible that the relationship between the phase of hyperpolarizing current input and the probability of subsequent spikes would also be observed in the hippocampal pyramidal cells, and affect the generation of place cell activity.

The MEC layer II excitatory neurons interact with each other primarily via inhibitory interneurons (Dhillon & Jones, 2000; Couey *et al.*, 2013), and rebound spikes might help to generate theta cycle skipping (Jeffery *et al.*, 1995; Deshmukh *et al.*, 2010) that is maintained as synchronous or antisynchronous firing in different sets of neurons (Brandon *et al.*, 2013). Our study of single-cell electrophysiology *in vivo* fills the gap between intrinsic properties shown by *in vitro* slice electrophysiology and grid cell activity in freely moving animals. Although we are unable to say that recorded cells are grid cells because of the use of anaesthetized mice, this result shows that rebound spikes *in vivo* may contribute to the spatial coding in MEC. Further experiments are needed to show the relationship between rebound spikes and grid cell activity with activation of the inhibitory network of MEC in freely moving animals.

Acknowledgements

This work was supported by NIMH R01 grants MH61492, MH60013, and ONR MURI N00014-10-1-0936. We would like to thank Dr Christopher F. Shay, Dr Michele Ferrante, and all members of the laboratory of M.E.H. for useful assistance and comments. We also thank Dr Hiroki Mutoh, Prof. Matt Wachowiak, Dr Takayuki Yamashita, Dr Christopher Schmidt-Hieber, and Prof. Jen-Wei Lin for technical assistance with *in vivo* patch-clamp recordings, and Professor Chantal E. Stern and Prof. Howard Eichenbaum for the use of laboratory resources. All authors have no conflict of interest in accordance with journal policy.

Abbreviations

kg bw, kg body weight; MEC, medial entorhinal cortex; MRA, mean resultant angle; MRL, mean resultant length.

References

Adhikari, M.H., Quilichini, P.P., Roy, D., Jirsa, V. & Bernard, C. (2012) Brain state dependent postinhibitory rebound in entorhinal cortex interneurons. *J. Neurosci.*, **32**, 6501–6510.

- Alonso, A. & Klink, R. (1993) Differential electroresponsiveness of stellate and pyramidal-like cells of medial entorhinal cortex layer II. *J. Neurophysiol.*, **70**, 128–143.
- Alonso, A. & Llinás, R.R. (1989) Subthreshold Na⁺-dependent theta-like rhythmicity in stellate cells of entorhinal cortex layer II. *Nature*, **342**, 175–177.
- Berens, P. (2009) CircStat: a MATLAB toolbox for circular statistics. *J. Stat. Softw.*, **31**, 1–21.
- Boccara, C.N., Sargolini, F., Thoresen, V.H., Solstad, T., Witter, M.P., Moser, E.I. & Moser, M.-B. (2010) Grid cells in pre- and parasubiculum. *Nat. Neurosci.*, **13**, 987–994.
- Brandon, M.P., Bogaard, A.R., Libby, C.P., Connerney, M.A., Gupta, K. & Hasselmo, M.E. (2011) Reduction of theta rhythm dissociates grid cell spatial periodicity from directional tuning. *Science*, **332**, 595–599.
- Brandon, M.P., Bogaard, A.R., Schultheiss, N.W. & Hasselmo, M.E. (2013) Segregation of cortical head direction cell assemblies on alternating theta cycles. *Nat. Neurosci.*, **16**, 739–748.
- Burgalossi, A., Herfst, L., von Heimendahl, M., Förste, H., Haskic, K., Schmidt, M. & Brecht, M. (2011) Microcircuits of functionally identified neurons in the rat medial entorhinal cortex. *Neuron*, **70**, 773–786.
- Cobb, S., Buhl, E., Halasy, K., Paulsen, O. & Somogyi, P. (1995) Synchronization of neuronal activity in hippocampus by individual GABAergic interneurons. *Nature*, **378**, 75–78.
- Couey, J.J., Witoelar, A., Zhang, S.-J., Zheng, K., Ye, J., Dunn, B., Czajkowski, R., Moser, M.-B., Moser, E.I., Roudi, Y. & Witter, M.P. (2013) Recurrent inhibitory circuitry as a mechanism for grid formation. *Nat. Neurosci.*, **16**, 318–324.
- Deshmukh, S.S., Yoganarasimha, D., Voicu, H. & Knierim, J.J. (2010) Theta modulation in the medial and the lateral entorhinal cortices. *J. Neurophysiol.*, **104**, 994–1006.
- Dhillon, A. & Jones, R.S. (2000) Laminar differences in recurrent excitatory transmission in the rat entorhinal cortex *in vitro*. *Neuroscience*, **99**, 413–422.
- Dickson, C.T., Magistretti, J., Shalinsky, M.H., Fransén, E., Hasselmo, M.E. & Alonso, A. (2000) Properties and role of I_h in the pacing of subthreshold oscillations in entorhinal cortex layer II neurons. *J. Neurophysiol.*, **83**, 2562–2579.
- Domnisoru, C., Kinkhabwala, A.A. & Tank, D.W. (2013) Membrane potential dynamics of grid cells. *Nature*, **495**, 199–204.
- Fernandez, F.R., Malerba, P., Bressloff, P.C. & White, J.A. (2013) Entorhinal stellate cells show preferred spike phase-locking to theta inputs that is enhanced by correlations in synaptic activity. *J. Neurosci.*, **33**, 6027–6040.
- Ferrante, M., Shay, C.F., Tsuno, Y., Chapman, W.G. & Hasselmo, M.E. (2014) Post-inhibitory rebound spikes in rat mec layer II/III principal cells: In-vivo, in-vitro, and in-silico evidence and characterization. *2014 Neuroscience Meeting Planner*, Program No. 297.11. Society for Neuroscience, Washington, DC.
- Giocomo, L.M., Zilli, E.A., Fransén, E. & Hasselmo, M.E. (2007) Temporal frequency of subthreshold oscillations scales with entorhinal grid cell field spacing. *Science*, **315**, 1719–1722.
- Gonzalez-Sulser, A., Parthier, D., Candela, A., McClure, C., Pastoll, H., Garden, D., Surmeli, G. & Nolan, M.F. (2014) GABAergic projections from the medial septum selectively inhibit interneurons in the medial entorhinal cortex. *J. Neurosci.*, **34**, 16739–16743.
- Haas, J.S. & White, J.A. (2002) Frequency selectivity of layer II stellate cells in the medial entorhinal cortex. *J. Neurophysiol.*, **88**, 2422–2429.
- Hafting, T., Fyhn, M., Molden, S., Moser, M.-B. & Moser, E.I. (2005) Microstructure of a spatial map in the entorhinal cortex. *Nature*, **436**, 801–806.
- Hahn, T.T.G., McFarland, J.M., Berberich, S., Sakmann, B. & Mehta, M.R. (2012) Spontaneous persistent activity in entorhinal cortex modulates cortico-hippocampal interaction *in vivo*. *Nat. Neurosci.*, **15**, 1531–1538.
- Hasselmo, M.E. (2014) Neuronal rebound spiking, resonance frequency and theta cycle skipping may contribute to grid cell firing in medial entorhinal cortex. *Philos. T. Roy. Soc. B*, **369**, 20120523.
- Hasselmo, M.E. & Shay, C.F. (2014) Grid cell firing patterns may arise from feedback interaction between intrinsic rebound spiking and transverse traveling waves with multiple heading angles. *Front. Syst. Neurosci.*, **8**, 201.
- Heys, J.G. & Hasselmo, M.E. (2012) Neuromodulation of I_h in layer II medial entorhinal cortex stellate cells: a voltage-clamp study. *J. Neurosci.*, **32**, 9066–9072.
- Heys, J.G., Giocomo, L.M. & Hasselmo, M.E. (2010) Cholinergic modulation of the resonance properties of stellate cells in layer II of medial entorhinal cortex. *J. Neurophysiol.*, **104**, 258–270.

- Hussaini, S.A., Kempadoo, K.A., Thuaud, S.J., Siegelbaum, S.A. & Kandel, E.R. (2011) Increased size and stability of CA1 and CA3 place fields in HCN1 knockout mice. *Neuron*, **72**, 643–653.
- Izhikevich, E.M. (2007) Chapter 7 & 8. *Dynamical Systems in Neuroscience: The Geometry of Excitability and Bursting*. MIT Press, Cambridge, Massachusetts, pp. 215–323.
- Jeffery, K.J., Donnett, J.G. & O'Keefe, J. (1995) Medial septal control of theta-correlated unit firing in the entorhinal cortex of awake rats. *NeuroReport*, **6**, 2166–2170.
- King, C., Recce, M. & O'Keefe, J. (1998) The rhythmicity of cells of the medial septum/diagonal band of Broca in the awake freely moving rat: relationships with behaviour and hippocampal theta. *Eur. J. Neurosci.*, **10**, 464–477.
- Kodandaramaiah, S., Franzesi, G. & Chow, B. (2012) Automated whole-cell patch-clamp electrophysiology of neurons in vivo. *Nat. Methods*, **9**, 585–587.
- Koenig, J., Linder, A.N., Leutgeb, J.K. & Leutgeb, S. (2011) The spatial periodicity of grid cells is not sustained during reduced theta oscillations. *Science*, **332**, 592–595.
- Lüthi, A. & McCormick, D.A. (1998) H-current: properties of a neuronal and network pacemaker. *Neuron*, **21**, 9–12.
- Margrie, T.W., Brecht, M. & Sakmann, B. (2002) In vivo, low-resistance, whole-cell recordings from neurons in the anaesthetized and awake mammalian brain. *Pflügers Arch.*, **444**, 491–498.
- McCormick, D.A. & Huguenard, J.R. (1992) A model of the electrophysiological properties of thalamocortical relay neurons. *J. Neurophysiol.*, **68**, 1384–1400.
- Quilichini, P., Sirota, A. & Buzsáki, G. (2010) Intrinsic circuit organization and theta-gamma oscillation dynamics in the entorhinal cortex of the rat. *J. Neurosci.*, **30**, 11128–11142.
- Ray, S., Naumann, R., Burgalossi, A., Tang, Q., Schmidt, H. & Brecht, M. (2014) Grid-layout and theta-modulation of layer 2 pyramidal neurons in medial entorhinal cortex. *Science*, **343**, 891–896.
- Richter, H., Klee, R., Heinemann, U. & Eder, C. (1997) Developmental changes of inward rectifier currents in neurons of the rat entorhinal cortex. *Neurosci. Lett.*, **228**, 139–141.
- Richter, H., Heinemann, U. & Eder, C. (2000) Hyperpolarization-activated cation currents in stellate and pyramidal neurons of rat entorhinal cortex. *Neurosci. Lett.*, **281**, 33–36.
- Sargolini, F., Fyhn, M., Hafting, T., McNaughton, B.L., Witter, M.P., Moser, M.-B. & Moser, E.I. (2006) Conjunctive representation of position, direction, and velocity in entorhinal cortex. *Science*, **312**, 758–762.
- Savelli, F. & Knierim, J.J. (2014) Strides toward a structure-function understanding of cortical representations of allocentric space. *Neuron*, **84**, 1108–1109.
- Schmidt-Hieber, C. & Häusser, M. (2013) Cellular mechanisms of spatial navigation in the medial entorhinal cortex. *Nat. Neurosci.*, **16**, 325–331.
- Shay, C.F., Boardman, I.S., James, N.M. & Hasselmo, M.E. (2012) Voltage dependence of subthreshold resonance frequency in layer II of medial entorhinal cortex. *Hippocampus*, **22**, 1733–1749.
- Shay, C.F., Ferrante, M., Chapman, G.W. & Hasselmo, M.E. (2015) Rebound spiking in layer II medial entorhinal cortex stellate cells: Possible mechanism of grid cell function. *Neurobiol. Learn. Mem.*, doi:10.1016/j.nlm.2015.09.004. [Epub ahead of print].
- Solstad, T., Boccara, C.N., Kropff, E., Moser, M.-B. & Moser, E.I. (2008) Representation of geometric borders in the entorhinal cortex. *Science*, **322**, 1865–1868.
- Sun, C., Kitamura, T., Yamamoto, J., Martin, J., Pignatelli, M., Kitch, L.J., Schnitzer, M.J. & Tonegawa, S. (2015) Distinct speed dependence of entorhinal island and ocean cells, including respective grid cells. *Proc. Natl. Acad. Sci. USA*, **112**, 9466–9471.
- Tang, Q., Burgalossi, A., Ebbesen, C.L., Ray, S., Naumann, R., Schmidt, H., Spicher, D. & Brecht, M. (2014) Pyramidal and stellate cell specificity of grid and border representations in layer 2 of medial entorhinal cortex. *Neuron*, **84**, 1191–1197.
- Tsuno, Y., Schultheiss, N.W. & Hasselmo, M.E. (2013) In vivo cholinergic modulation of the cellular properties of medial entorhinal cortex neurons. *J. Physiol.*, **591**, 2611–2627.
- Varga, V., Hangya, B., Kránitz, K., Ludányi, A., Zemankovics, R., Katona, I., Shigemoto, R., Freund, T.F. & Borhegyi, Z. (2008) The presence of pacemaker HCN channels identifies theta rhythmic GABAergic neurons in the medial septum. *J. Physiol.*, **586**, 3893–3915.
- Yoshida, M., Giocomo, L.M., Boardman, I. & Hasselmo, M.E. (2011) Frequency of subthreshold oscillations at different membrane potential voltages in neurons at different anatomical positions on the dorsoventral axis in the rat medial entorhinal cortex. *J. Neurosci.*, **31**, 12683–12694.
- Zemankovics, R., Káli, S., Paulsen, O., Freund, T.F. & Hájos, N. (2010) Differences in subthreshold resonance of hippocampal pyramidal cells and interneurons: the role of h-current and passive membrane characteristics. *J. Physiol.*, **588**, 2109–2132.